

Dislocation processes during the plastic deformation of γ -TiAl

D. HÄUSSLER[†], M. BARTSCH[†], M. AINDOW[‡], I. P. JONES[‡]
and U. MESSERSCHMIDT^{†§}

[†] Max Planck Institute of Microstructure Physics, Weinberg 2, Halle/Saale,
D-06120, Germany

[‡] School of Metallurgy and Materials and Interdisciplinary Research Centre in
Materials for High Performance Applications, University of Birmingham,
Birmingham B15 2TT, England

[Received 4 March 1998 and accepted in revised form 1 July 1998]

ABSTRACT

In situ straining experiments in a high-voltage electron microscope have been performed on coarse-grained γ -Ti–52 at.% Al at room temperature and elevated temperatures, in addition to macroscopic compression tests. At all temperatures examined, ordinary dislocations, superdislocations of $\langle 101 \rangle$ Burgers vectors and microtwins carry the deformation, with ordinary dislocations dominating. The processes controlling the deformation differ greatly for the temperature ranges below and above about 850 K. At low temperatures, ordinary dislocations as well as superdislocations move jerkily between positions where they are locally pinned, which can best be described by a precipitation-hardening mechanism. At high temperatures, the $\langle 101 \rangle$ superdislocations show a shape typical of the locking–unlocking mechanisms. The ordinary dislocations are created and move in a very instantaneous event. Later, they are smoothly curved and move in a viscous way. The nonplanar arrangement of these dislocations indicates the importance of diffusion processes. The dynamic behaviour and the results of macroscopic deformation tests are explained by the formation of intrinsic atmospheres around the dislocations.

§1. INTRODUCTION

Titanium aluminides are prospective materials for structural applications owing to their light weight, the relatively good corrosion resistance and, particularly, their high flow stress up to temperatures above 900 K. The latter is due to the so-called flow stress anomaly, that is an increase in or, at least, a constancy of the flow stress with increasing temperature over a wide range. The flow stress anomaly is characteristic also of other intermetallic materials.

Materials of technological interest on the basis of TiAl are mostly two-phase ($\alpha_2 + \gamma$) alloys. Single-phase γ alloys have some major disadvantages regarding their room-temperature formability, their creep and also their strength properties. However, in two-phase alloys the major part of plastic deformation occurs in the γ phase so that the single-phase γ alloys may serve as a model material of the plastic constituent of other TiAl materials. For a comprehensive review of recent research on γ -TiAl-based materials, see Yamaguchi *et al.* (1995).

The γ phase of TiAl is of $L1_0$ structure, which is characterized by lattice planes alternately occupied by Al and Ti atoms. Consequently, the $\{111\}$ slip planes consist

§ Author for correspondence. Email, um@mpi-halle.mpg.de.

of separate rows of Al and Ti atoms in the $\langle 110 \rangle$ directions. According to the atomic arrangement in the γ phase and its weak tetragonality ($c/a \approx 1.02$), there exist three types of dislocation with different Burgers vectors, namely ordinary dislocations with $\mathbf{b}_o = \frac{1}{2}\langle 110 \rangle$, superdislocations with $\mathbf{b}_{s1} = \langle 101 \rangle$, and superdislocations with $\mathbf{b}_{s2} = \frac{1}{2}\langle 112 \rangle$. In addition to dislocation motion, γ -TiAl may also deform by twinning.

Several attempts have been made to explain the deformation behaviour of TiAl, and particularly its flow stress anomaly. As reviewed by Vitek (1992), the core structure markedly influences the properties of dislocations in ordered non-cubic phases. The following mechanisms of the temperature dependence of the flow stress may be discussed.

- (1) As the energy of the planar faults on the $\{100\}$ plane is lower than on the $\{111\}$ plane, dissociated superdislocations with $\mathbf{b}_{s1} = \langle 101 \rangle$ may cross-slip from the $\{111\}$ slip plane to the $\{100\}$ cross-slip plane where they become locked (Hug *et al.* 1988) similarly to the situation in $L1_2$ alloys (Kear and Wilsdorf 1962). In a more general way, the cores of the dislocations either may extend on their slip plane, resulting in a glissile configuration, or may assume a three-dimensional structure, leading to a low mobility. This refers to superdislocations (for example Girshick and Vitek (1995) and Panova and Farkas (1995)) as well as to ordinary dislocations (Girshick and Vitek 1995, Panova and Farkas 1995, Simmons *et al.* 1997). Experimental observations show that the cores of ordinary dislocations should be rather compact (Simmons *et al.* 1995).
- (2) Dislocations can be trapped in deep Peierls valleys (for example Greenberg *et al.* (1991)).
- (3) The pinning–unzipping model described by Viguier *et al.* (1995) and Louchet and Viguier (1995) is based on local cross-slip of ordinary screw dislocations on different $\{111\}$ planes. The resulting dislocation configuration is not planar so that the dislocation cannot glide on a single plane. Recent results from electron microscopy by Sriram *et al.* (1997) showed that the segments of ordinary dislocations bow out on parallel planes.

In the models, either different core structures of dislocations are assumed at different temperatures, or locking or pinning as well as unlocking or unpinning are considered thermally activated so that a higher rate of locking or pinning at higher temperatures may explain the flow stress anomaly. The different mechanisms are based on the different types of dislocation, namely ordinary dislocations or superdislocations. Consequently, a number of transmission electron microscopy studies have been carried out to assess the contributions of the different dislocation types at different temperatures. While some workers mainly observed superdislocations at room temperature (for example, Court *et al.* (1990)) others found a dominance of ordinary dislocations at all temperatures (for example Morris (1996)). Apparently, the activation of the different types of dislocation depends on the concentration of O impurities within the specimens (Aindow *et al.* 1990, Kad and Fraser 1994, Morris 1996) as well as on the Al content (Inui *et al.* 1997).

In-situ deformation experiments in a transmission electron microscope, where moving dislocations can directly be observed, may essentially contribute to establish the relevant deformation mechanisms. Such experiments on single-phase γ -TiAl have been reported by Farenc *et al.* (1991, 1993), Farenc and Couret (1993), Caillard *et al.* (1993) and Caillard (1995). The present paper describes *in-situ* straining experiments

on γ -TiAl in a high-voltage electron microscope, which allows the observation of thicker specimens, which better represent bulk-like properties. These observations of the dynamic behaviour of individual dislocations are supplemented by macroscopic deformation tests. It is hoped that the results will contribute to better understanding of the processes controlling the flow stress of TiAl. Preliminary results were published earlier by Messerschmidt *et al.* (1995) and Häussler *et al.* (1995).

§2. EXPERIMENTAL DETAILS

The single-phase alloy investigated was melted in a cold-hearth two-torch plasma arc furnace. It is coarse-grained, consisting of Ti-52 at.% Al with an O content of about 750 at.ppm. The microtensile specimens for the *in-situ* straining experiments were prepared by cutting, grinding and two-step jet polishing between platinum masks using an electrolyte consisting of methanol, butanol and perchloric acid (233 K; 20 V). Usually, the central region of the strip-shaped specimens showed large transparent regions around one or several perforations. Because of the large grains, the active gauge length of the *in-situ* specimens consisted of a single crystal.

The experiments were carried out in quantitative straining stages, either for room temperature or for grip temperatures up to 1520 K, at a maximum load of 15 N (Messerschmidt and Appel 1976, Messerschmidt and Bartsch 1994). The high-voltage electron microscope was operated at 1 MeV. The deformation was performed in small load increments such that the changes in the microstructure under full load could be recorded either on photographic film or on video tape. In order to minimize unavoidable radiation damage during the *in-situ* experiment, usually the dislocation structures were characterized in more detail in the unloaded state in a wide-angle goniometer at room temperature.

The validity of the results of *in-situ* straining experiments is generally limited by the low thickness of the specimens even in the high-voltage electron microscope and by the radiation damage inside the latter. The dislocation length of more than 0.8 μm should be sufficient to show the bulk dynamical behaviour of individual dislocations. Electron damage may cause disordering of the γ phase. However, Hishinuma *et al.* (1993) proved this material to be quite resistant to electron radiation, showing a low growth rate of defect clusters and a weak tendency of void formation.

Macroscopic compression tests were performed in an Instron 8562 single-screw testing machine. Deformation curves were measured at a constant strain rate and temperature. The strain rate sensitivity I of the flow stress was determined by strain-rate cycling and stress relaxation experiments. During the latter, the plastic strain rate $\dot{\epsilon}_{\text{plast}}$ is proportional to the negative stress rate $-\dot{\sigma}$, yielding

$$I = \frac{\Delta\sigma}{\Delta(\ln \dot{\epsilon}_{\text{plast}})} = \frac{\Delta\sigma}{\Delta[\ln(-\dot{\sigma})]} \quad (1)$$

§3. RESULTS OF *IN-SITU* STRAINING EXPERIMENTS

3.1. Room temperature

Apart from some twinning, room-temperature deformation is mainly carried by dislocations, mostly ordinary dislocations of Burgers vector $\mathbf{b}_0 = \frac{1}{2}\langle 110 \rangle$ as in figure 1, and occasionally by superdislocations with $\mathbf{b}_{s1} = \langle 101 \rangle$ as in figure 2. Superdislocations with Burgers vectors of the type $\mathbf{b}_{s2} = \frac{1}{2}\langle 112 \rangle$ have not been observed. The majority of dislocations move on $\{111\}$ planes and are of screw

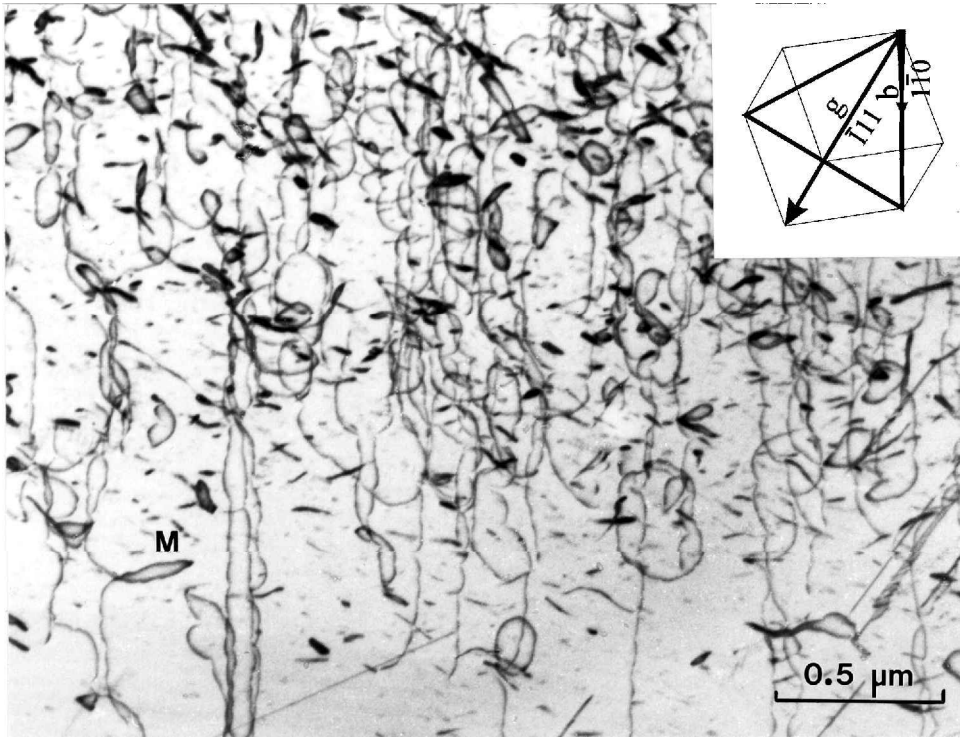


Figure 1. Dislocation structure under load during *in-situ* deformation at room temperature. Most dislocations are ordinary dislocations near the screw orientation. In this and the following figures, the pictograms mark the orientation of the Thompson tetrahedron, sometimes inserted in the cube. Arrows with wedge-shaped shafts label Burgers vectors inclined to the image plane.

character. In only one case, stereo images proved a slip band of ordinary dislocations to have moved on $\{110\}$ planes. In the *in-situ* experiments, the moving dislocations may trail slip traces which appear as weak lines as, for example, in figure 2. Slip traces ending at a dislocation indicate that the dislocation had moved during the *in-situ* experiment. Most dislocations move in slip bands. The dislocation density within these bands is in the order of magnitude of $(1-3) \times 10^{13} \text{ m}^{-2}$.

Figure 1 presents a section of such a slip band showing the typical shape of ordinary dislocations during the *in-situ* experiments under full load. All dislocations are of curly shape, indicating that the dislocation motion is impeded by obstacles between which the dislocation segments bow out under stress. In most cases, the obstacle sites are not aligned accurately in screw direction but are distributed over the slip plane. In order to determine the spatial arrangement of the bowed-out dislocation segments, some stereo pairs of the dislocation structure were taken under load, and some others in the unloaded state after the *in-situ* experiment, as in figure 3. Both kinds of stereo pair reveal that most of the segments bow out on a single slip plane or on parallel planes respectively. Some, however, bow out on other planes, too. In these cases, usually always groups of neighbouring segments bow out again on parallel planes. The obstacles with deep cusps are clearly jogs, some of which are labelled J in figure 3. The jogs trailing dipoles (dislocation debris) are labelled D. The dipoles are arranged in several crystallographic directions, usually

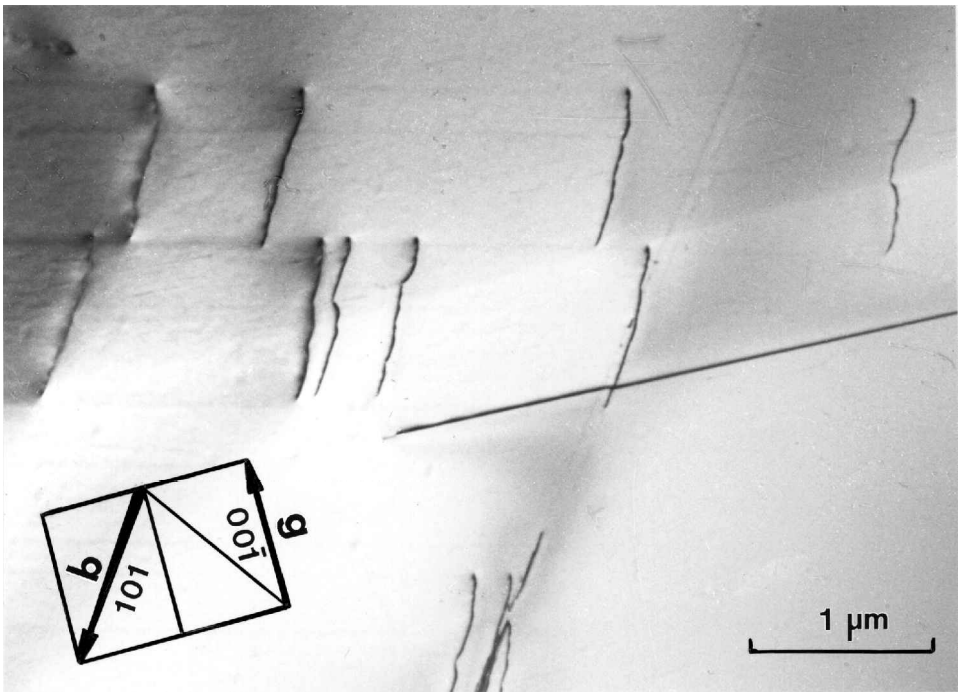


Figure 2. Head of a slip band of superdislocations with $\langle 101 \rangle$ Burgers vector. (After Messerschmidt *et al.* (1995).)

not in edge direction. Some of them are oriented in $\langle 101 \rangle$ directions, that is they are of 60° character. If the jogs are high enough, both arms of the dipole may pass each other as at M in figure 1, leading to dislocation multiplication. Only a few micrographs are available, showing edge dislocation segments. Under load, edge dislocations reveal the same curly shape as screw dislocations, as demonstrated in figure 4. When the specimen is unloaded, the bowed-out segments relax only weakly, revealing the curly shape also in the unloaded state, as shown in figure 3. Figure 2 illustrates that superdislocations with $\mathbf{b}_{s1} = \langle 101 \rangle$ are pinned like the ordinary dislocations. However, their bowing is always less strong. Slip traces prove that these dislocations had moved during the *in-situ* experiment. In conclusion, it may be pointed out that obstacles impede the motion of all dislocations, regardless of whether they are ordinary dislocations or superdislocations, and independent of their character, that is screw or edge. In order to identify the structure of the obstacles, specimens have been examined by high-resolution electron microscopy lattice imaging and by electron-energy-loss spectroscopy. Although inhomogeneities of the structure were observed, it has not yet been possible to identify clearly the nature of the obstacles.

Video recordings reveal the kinematic behaviour of the moving dislocations. Ordinary dislocations move jerkily as the four different stages in figure 5 demonstrate. In the forward direction, the dislocations always advance a small segment, indicated by white arrows, which afterwards spreads laterally. Figure 5(d) shows two successive positions of a dislocation segment in the same video frame. Thus, this segment has jumped within the time of one frame ($\frac{1}{50}$ s). At low average velocities, moving single dislocations sweep areas of the order of magnitude of the square of the obstacle distance as concluded from video recordings. At higher velocities, the

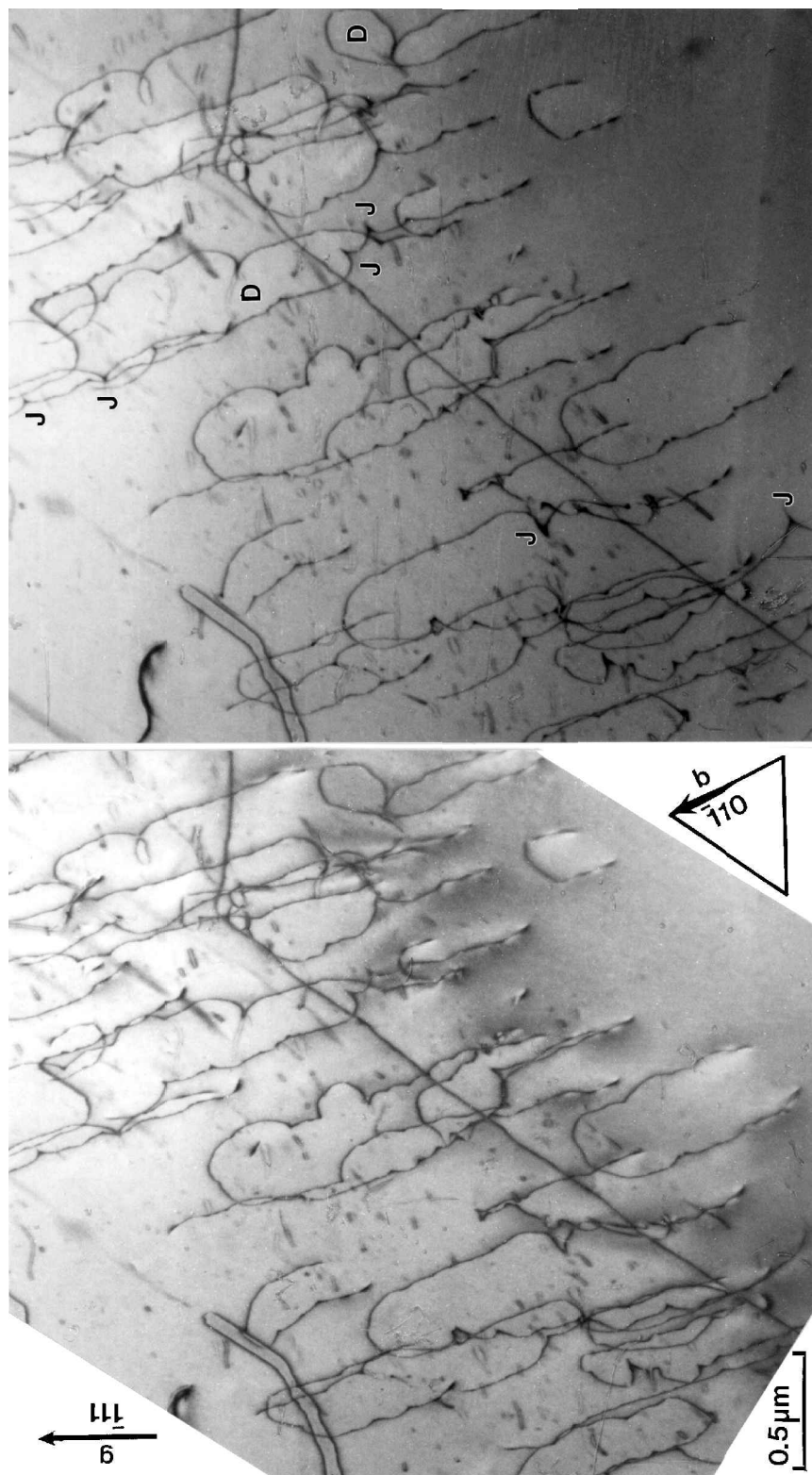


Figure 3. Stereo pair of a slip band taken in a wide-angle goniometer after an *in-situ* experiment at room temperature.

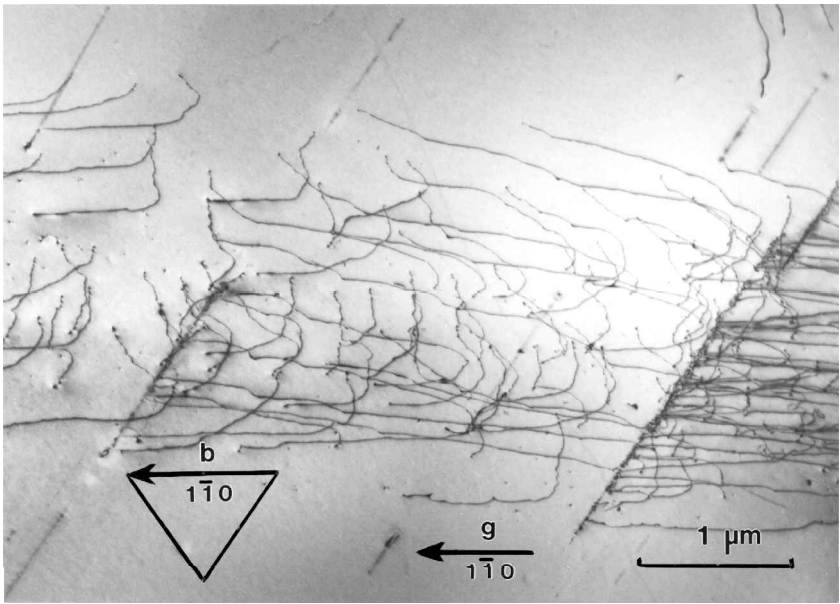


Figure 4. Slip band taken during *in-situ* deformation at room temperature showing ordinary mixed and edge dislocations. The traces in the $[112]$ directions are traces of defects on (111) planes, probably twins. The ordinary dislocations are created at these defects. The indicated Burgers vector $\mathbf{b}_o = \frac{1}{2}[110]$ is the only possible Burgers vector of ordinary dislocations in this micrograph.

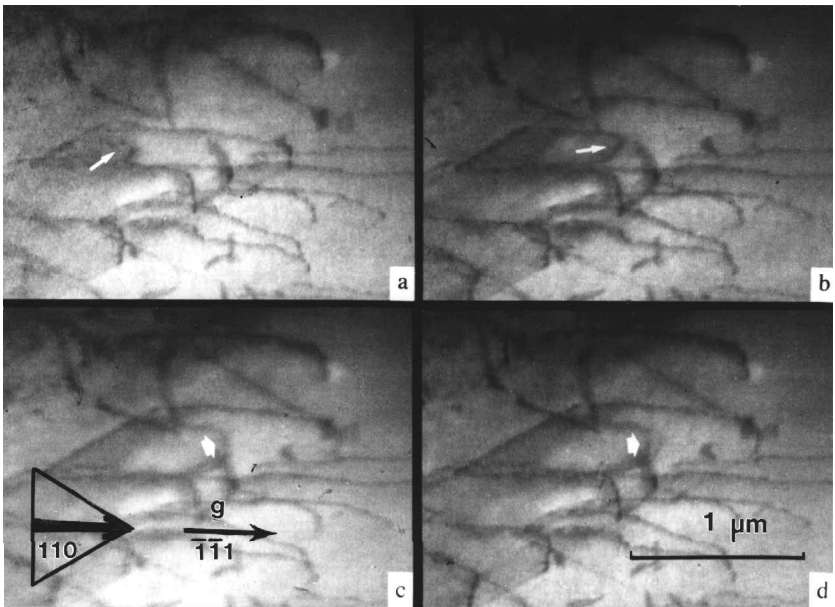


Figure 5. Motion of ordinary dislocations at room temperature. The four stages are taken from a video recording. Always small segments labelled by white arrows are pushed forwards and later spread sideways. In (d), the segment labelled by a white arrow is imaged twice, that is it moved jerkily within the time of a single video frame ($\frac{1}{30}$ s).

dislocations jump over longer distances of the order of magnitude of $1\ \mu\text{m}$, or more. In slip bands, several dislocations may move collectively. The dynamic behaviour of ordinary dislocations is independent of their character, that is it is the same for screw and edge dislocations. Superdislocations have never been observed during their motion. It may therefore be concluded that they move very jerkily over long distances.

In order to obtain quantitative data on the obstacle mechanism, the distances l between the pinning points were measured along the dislocations. As shown in table 1, for ordinary dislocations as well as for superdislocations the average values are always around 100 nm. Figure 6 presents a histogram of the obstacle distances along

Table 1. Obstacle distances l between the pinning points.

T/K	Burgers vector	Character	l/nm	Number of segments
295	$\mathbf{b}_o = \frac{1}{2}\langle 110 \rangle$	screw	105	1800
295	$\mathbf{b}_o = \frac{1}{2}\langle 110 \rangle$	mixed or edge	73	350
295	$\mathbf{b}_{s1} = \frac{1}{2}\langle 101 \rangle$	screw	95	640
665	$\mathbf{b}_o = \frac{1}{2}\langle 110 \rangle$	screw	90	715
665	$\mathbf{b}_o = \frac{1}{2}\langle 110 \rangle$	mixed or edge	100	285

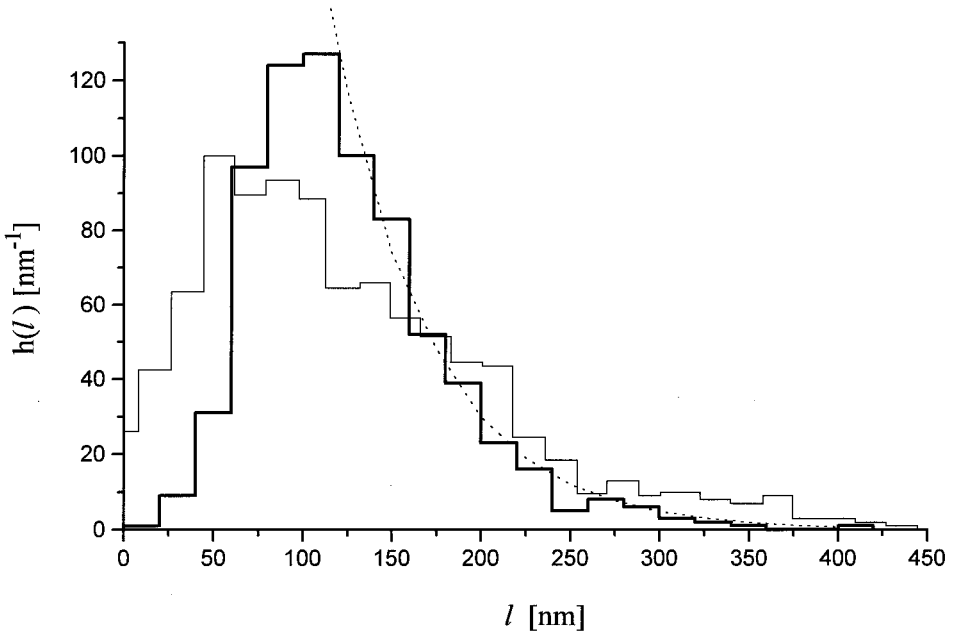


Figure 6. Frequency distribution of the obstacle distances along screw dislocations at room temperature (bold line). Data were taken from one micrograph. The dotted curve shows the exponential distribution according to the model described by Louchet and Viguier (1995) fitted to the decreasing part of the experimental distribution. This curve violates the normalization condition. The thin line shows the theoretical distribution for precipitation hardening according to computer simulation experiments from the paper by Appel *et al.* (1982). The distribution is scaled to the mean value of the experimental distribution.

screw dislocations together with two theoretical curves. It has a typical asymmetric shape. The stress τ_e corresponding to an equilibrium curvature of the bowed-out dislocation segments was determined by fitting the shape of the segments calculated by the line tension theory of elastically anisotropic materials to the shape in the micrographs. The line tension data used were calculated by M. H. Yoo (1994, private communication) based on the theoretical elastic constants of Fu and Yoo (1990). The theoretical equilibrium shapes of loops under stress are shown in figure 7. While ordinary dislocations are of almost circular shape, superdislocations are elliptic, with their screw segments showing a very low curvature. The theoretical curves were plotted with different sizes in the projections of the electron micrographs and matched with the shapes of the bowed-out dislocation segments. The reciprocal value S of the major half-axis of the fitting loops was taken as a measure of the curvature of the segments as described by Messerschmidt (1993) for other materials. The value of S is related to the stress τ_e by

$$\tau_e = \frac{b}{4\pi} K_e S \{ \ln(l/r_0) + C \}, \quad (2)$$

where b is the absolute value of the Burgers vector, K_e is the energy constant of the edge dislocation (which, according to M. H. Yoo (1994, private communication), is equal to 84 GPa for ordinary dislocations, and to 99 MPa for superdislocations with $\langle 101 \rangle$ Burgers vectors), l is the obstacle distance of the individual segments,

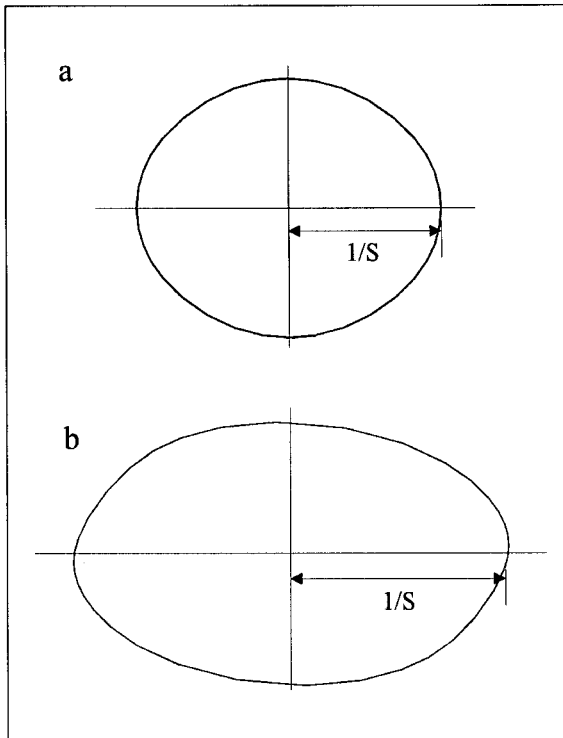


Figure 7. Shape of (a) ordinary dislocations with $\mathbf{b}_o = \frac{1}{2}\langle 110 \rangle$ and (b) superdislocations with $\mathbf{b}_{s1} = \langle 101 \rangle$, calculated by the line tension model using elastic anisotropy. (Data from M. H. Yoo (1994, private communication).)

Table 2. Local effective stress τ_c at room temperature, determined from dislocation curvature.

Burgers vector	Character	τ_c /MPa	Number of segments
$\mathbf{b}_o = \frac{1}{2}\langle 110 \rangle$	screw	40	40
$\mathbf{b}_{s1} = \langle 101 \rangle$	screw	37	30
$\mathbf{b}_{s1} = \langle 101 \rangle$	edge	40	15

$r_0 = b_o = 0.282$ nm is the inner cut-off radius and $C = -1.61$ is a numerical constant. The latter takes into account the curly shape of dislocations (estimated from the work of Scattergood and Bacon (1975)). The results of the evaluation are listed in table 2. Ordinary dislocations and superdislocations indicate the same value of the effective stress. It is important to note that, as described above, the dislocation bowing only slightly relaxes after unloading.

3.2. High temperatures

In addition to the experiments at room temperature, a number of *in-situ* straining experiments were performed between about 665 and 1050 K. These temperatures correspond to the range of peak stresses before the high-temperature decrease in the flow stress starts.

Two experiments were carried out at intermediate temperatures, namely at about 665 and 850 K. Similarly to room temperature, deformation occurs by the motion of ordinary dislocations and superdislocations as well as by twinning. Figure 8 shows ordinary dislocations moving during the deformation at 665 K. The different width of the slip traces, for example of dislocations A and B, indicates that the dislocations must have large jogs. They cause a wide variation in the slip trail width because of the flat inclination of the slip planes. In spite of the jogs, the dislocations are quite smooth, that is the extent of bowing is drastically reduced compared with that at room temperature so that the cusps in the dislocation line corresponding to the obstacles are scarcely visible. Nevertheless, the average obstacle distance listed in table 1 is still approximately equal to its room temperature value. Most of the dislocations in figure 8 are additionally pinned at the surfaces of the specimen, probably owing to an oxide layer. The kinematic behaviour of the dislocations at 665 K is similar to that at room temperature. Figure 9 shows ordinary dislocations taken during an *in-situ* experiment at 850 K. The number of cusps is strongly decreased. The dislocations are pinned by only a few jogs about 0.5–1 μm apart.

A number of experiments were performed at temperatures between 870 and 930 K, and one experiment at about 1050 K. The shape as well as the dynamic behaviour of dislocations have changed strongly with respect to those at lower temperatures. The obstacles, which affect the motion of all dislocations at room temperature and at intermediate temperatures, no longer act above about 870 K. As demonstrated in figure 10, the ordinary dislocations with $\mathbf{b}_o = \frac{1}{2}\langle 110 \rangle$ Burgers vectors are smoothly bent with large radii of curvature. A nonplanar arrangement shows that their motion is not restricted to their slip planes. In addition to the predominant curved dislocation segments, some segments are straight and arranged in $\langle 101 \rangle$ direction. They are the only segments lying on the original (111) slip plane. The spatial arrangement of the dislocations is proved by several stereo pairs taken after the *in-situ* experiments at room temperature. A section of one of them is shown

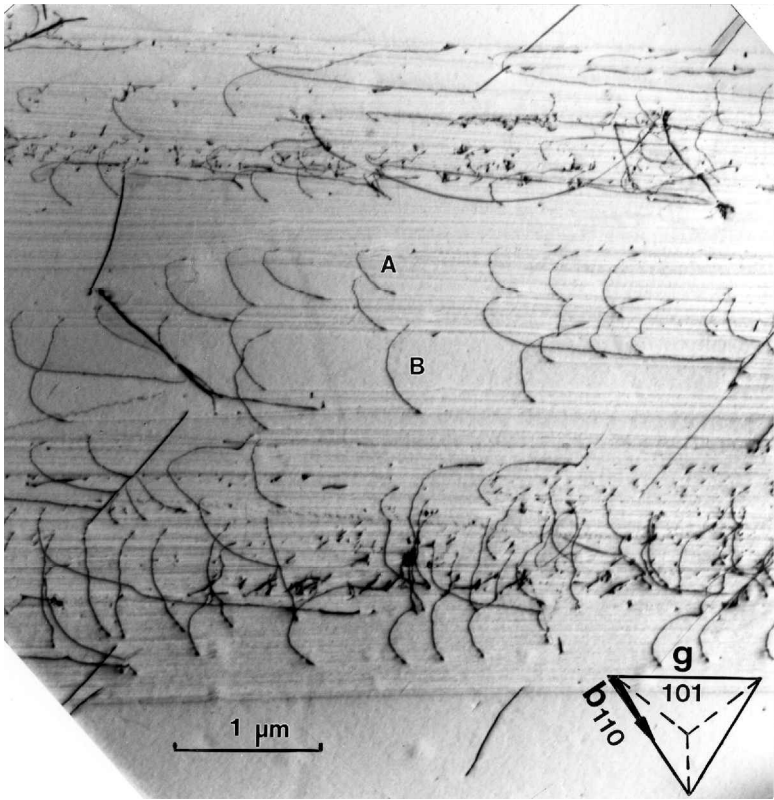


Figure 8. Ordinary screw dislocations moving during *in-situ* straining at 665 K.

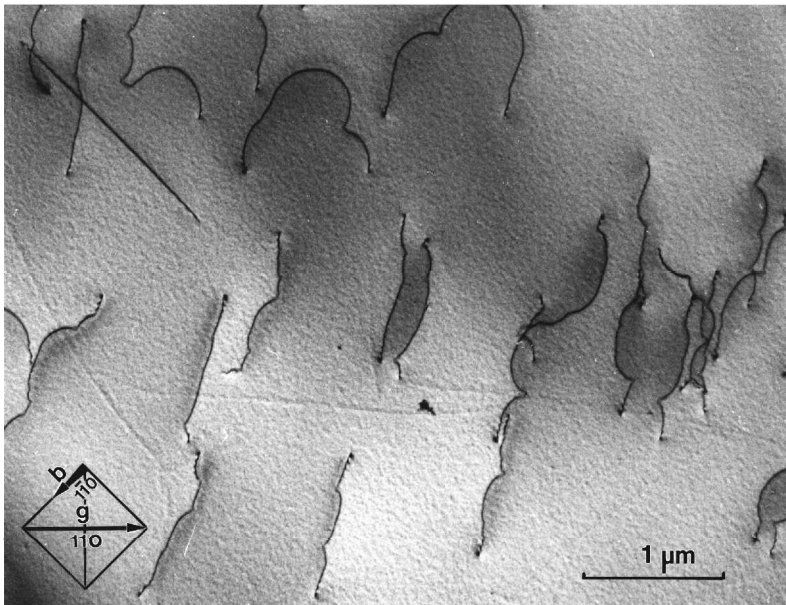


Figure 9. Ordinary dislocations moving during *in-situ* deformation at 850 K.

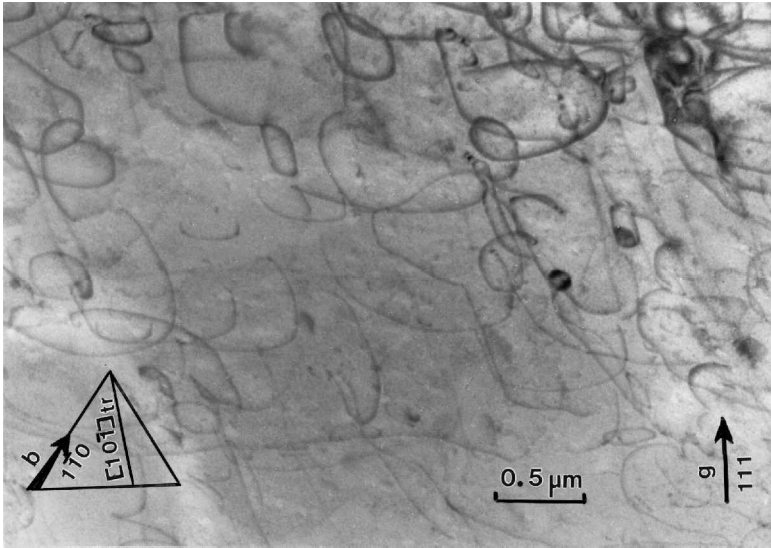


Figure 10. Ordinary dislocations imaged under load during *in-situ* straining at 930 K. (After Häussler *et al.* (1995).)

in figure 11. Owing to unloading and cooling, the dislocation structure may be slightly relaxed compared with that during *in-situ* straining. Superdislocations with $\langle 101 \rangle$ Burgers vectors also occur less frequently at elevated temperatures than simple dislocations do. Figure 12 shows that they are characterized by long segments oriented along a $\langle 110 \rangle$ direction linked by segments in the two other $\langle 110 \rangle$ directions on the respective $\{111\}$ slip plane. Thus, these dislocations are not of screw type.

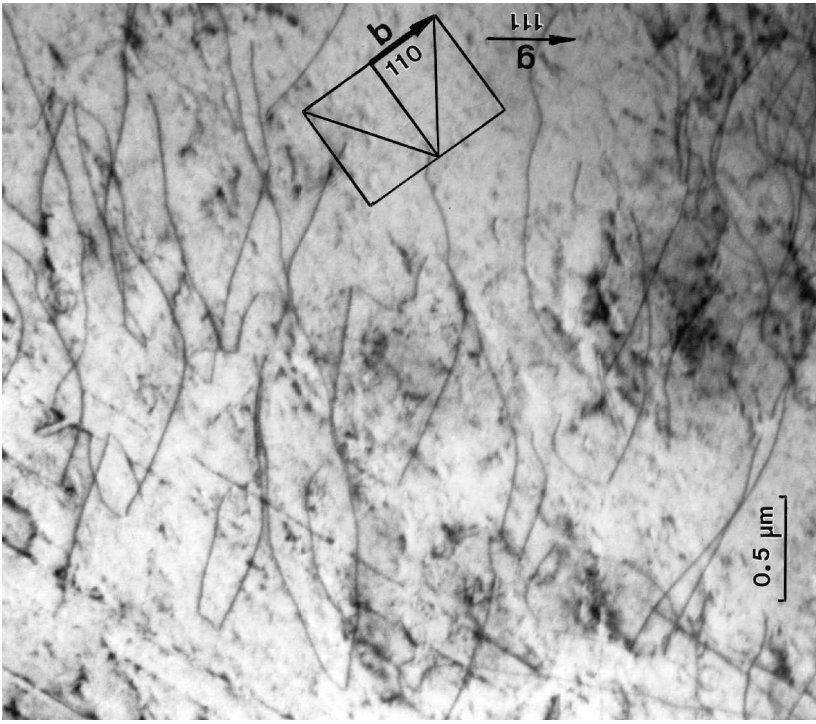
On loading the specimens for the first time during the *in-situ* experiments above about 870 K, large numbers of ordinary dislocations and some superdislocations usually appear instantaneously at a certain load. If ordinary dislocations again start to move, their motion is no longer jerky but smooth in a viscous way. The movement of superdislocations with $\mathbf{b}_{s1} = \langle 101 \rangle$ has never been recorded. Obviously, they jump over larger distances before they become locked again.

Dislocation debris appears in the form of small dislocation loops instead of dipoles, which appear at lower temperatures.

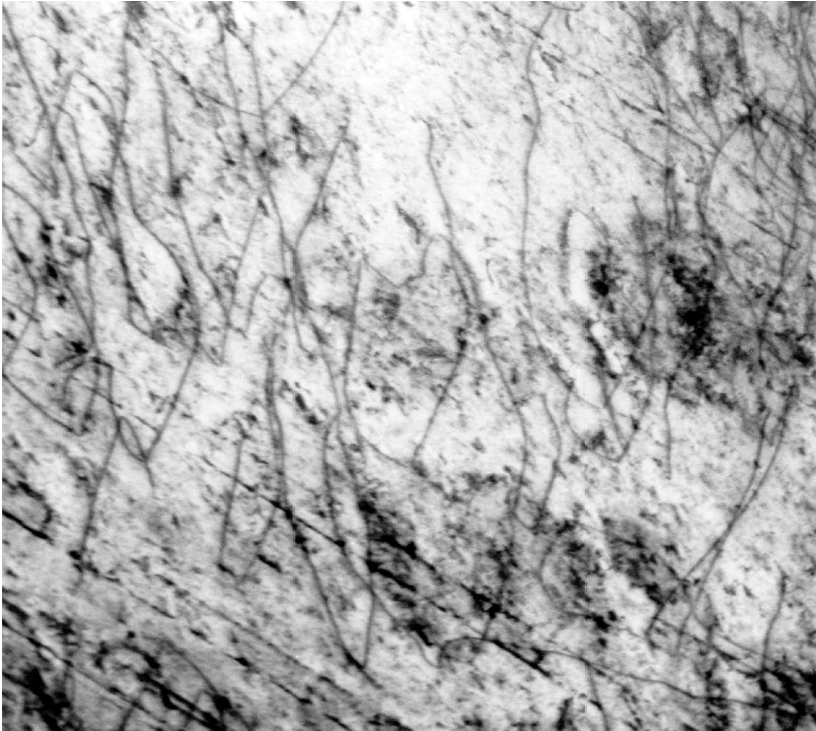
§4. RESULTS OF MACROSCOPIC DEFORMATION TESTS

Table 3 summarizes the results of compression tests performed at different temperatures at a strain rate of 10^{-5} s^{-1} using the same piece of material as in the *in-situ* experiments. The flow stress σ_0 is obtained by linearly extrapolating the hardening range onto a straight line representing the elastic range. The activation volume is given by $V = \alpha kT/I$. $\alpha = 3$ is the Taylor factor. σ_0 as well as V increase slightly with increasing temperature.

Four additional compression tests were performed on a second piece of material of the same composition and treatment, using different strain rates between about 840 and 970 K in order to characterize the dynamic deformation behaviour in more detail. Figure 13 shows a stress relaxation curve representing more than three orders of magnitude of the strain rate. This curve shows a typical 'inverse' curvature with a low strain-rate sensitivity I (inverse slope) at high stresses, and a higher strain-rate



(b)



(a)

Figure 11. Stereo pair of the structure of ordinary dislocations produced during *in-situ* deformation at 930 K imaged post mortem at room temperature.

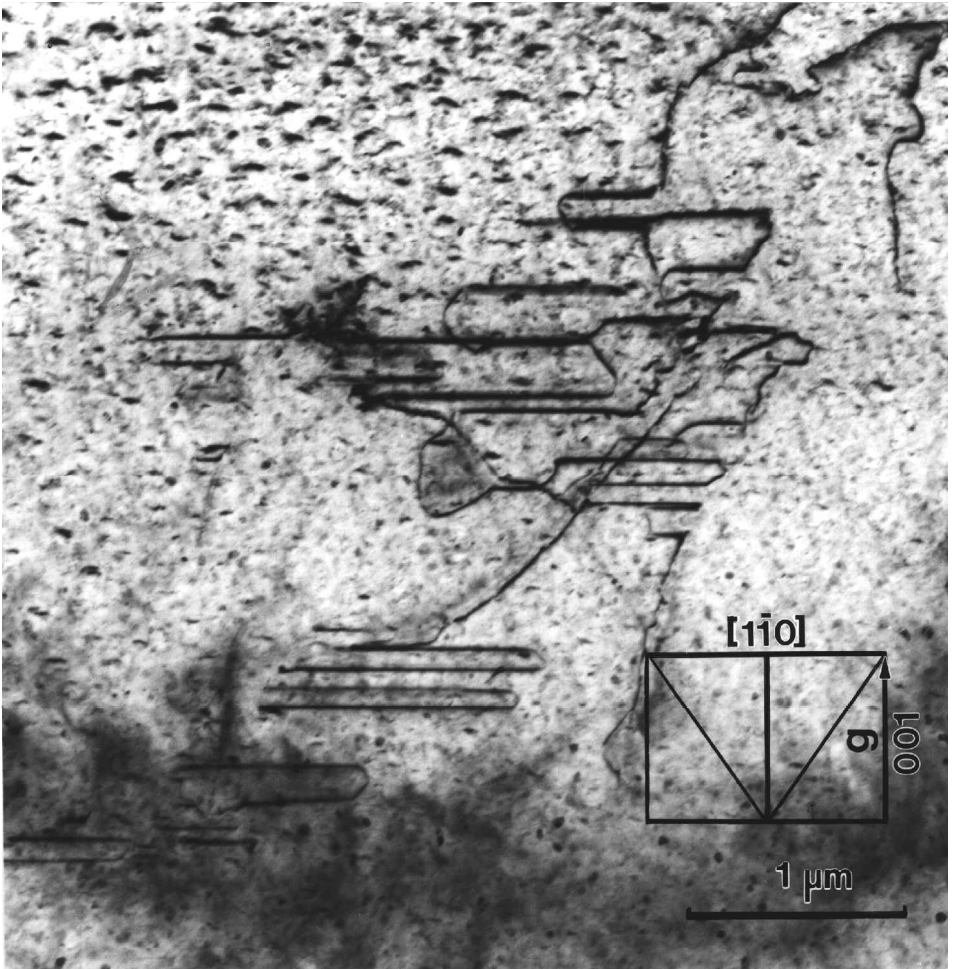


Figure 12. Superdislocations with $\mathbf{b}_{s1} = \langle 101 \rangle$ under load which have moved at 930 K.

sensitivity at lower stresses. The strain-rate sensitivities were determined at different points along the relaxation curves and then plotted against the actual strain rate. The latter was obtained from the stress rate using the stiffness of the sample and fixtures during unloading at the end of the experiments. Data from one experiment at 990 K are plotted in figure 14. The strain-rate sensitivity decreases strongly down to small values with increasing strain rate. It increases quite strongly with increasing strain and only weakly with decreasing temperature. The relaxation curve in figure 13 also

Table 3. Average values of flow stress σ_0 , straining rate sensitivity I and activation volume V at different temperatures.

T/K	σ_0/MPa	I/MPa	V/nm^3
294	175 ± 10	0.9	13.5
673	215 ± 10	1.4	19.8
862	225 ± 10	1.6	22.4

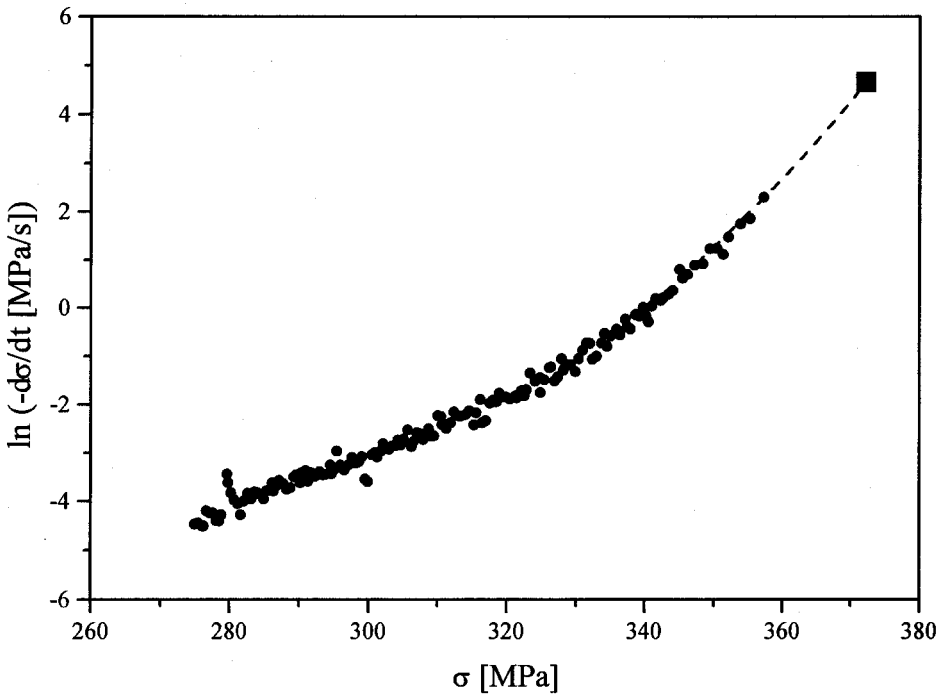


Figure 13. Stress relaxation curve taken at 900 K.

demonstrates that only a small part of the total flow stress relaxes during usual relaxation times (about 10 min).

§ 5. DISCUSSION

Although the present single-phase γ -TiAl material shows almost identical flow stresses and activation volumes over the whole temperature range investigated, the dislocation processes differ greatly between room temperature and high temperatures. Nevertheless, the microstructure is always characterized by the presence of ordinary dislocations, superdislocations and microtwins. Twinning is not discussed here, since it was of minor importance in the *in-situ* experiments and since there is a detailed paper about it by Farenc *et al.* (1993). The present experiments do not allow a detailed analysis of the relative contributions of the different microprocesses. A study of these has been published recently by Inui *et al.* (1997). However, in the present *in-situ* experiments, ordinary dislocations dominate at all temperatures. This may be due to the lower Al content than in the work by Inui *et al.* (1997).

5.1. From room temperature up to about 700 K

The essential experimental observations in the low-temperature range are as follows:

- (1) The density of ordinary dislocations is much higher than that of superdislocations with $\langle 101 \rangle$ Burgers vectors.
- (2) Of the two types, screw dislocations dominate during the *in-situ* deformation.

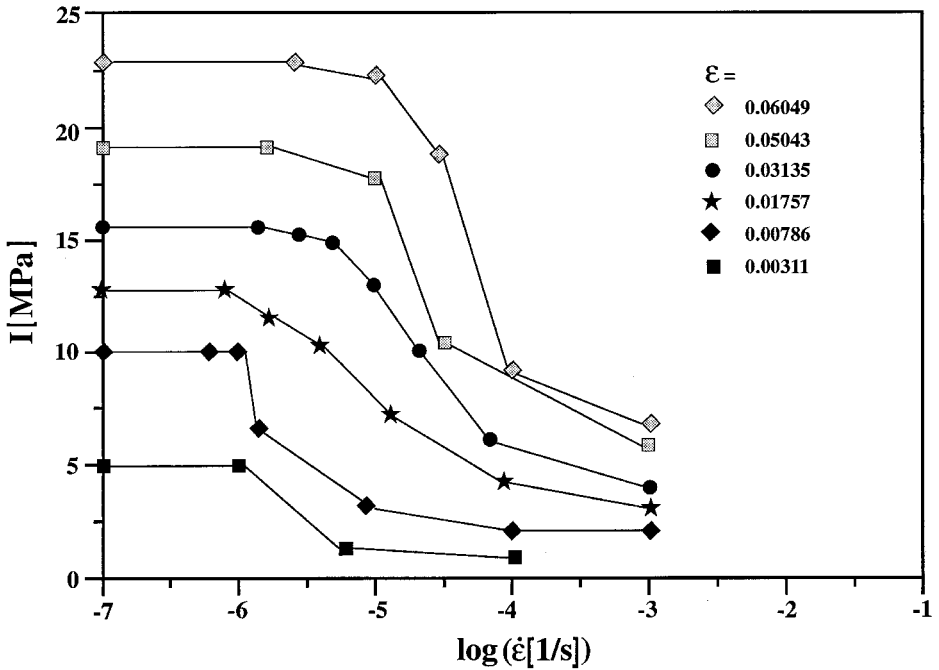


Figure 14. Strain-rate sensitivity I at 970 K as a function of the strain rate $\dot{\epsilon}$ with the strain as parameter.

- (3) Dislocations of both types bow out between obstacles to form cusps in the dislocation lines.
- (4) These cusps are not exactly aligned along the screw orientation but are spread on the slip plane.
- (5) Cusps appear also on mixed and edge ordinary dislocations.
- (6) Neighbouring segments of ordinary dislocations bow out on the same $\{111\}$ plane, or on parallel planes.
- (7) The obstacle distance amounts to about 100 nm over the whole range between room temperature and about 700 K.
- (8) Under stress, the bowing decreases with increasing temperature.
- (9) The bowing does not relax significantly after unloading.
- (10) Independent of their character, that is screw or edge, ordinary dislocations move by advancing a segment of the length of one or a few obstacle distances followed by the sideways spreading of the advanced segment. At high velocities, the dislocations move jerkily over distances of some micrometers.
- (11) Superdislocations have never been observed to move, that is they move in a very jerky manner.

The superdislocations with $\langle 101 \rangle$ Burgers vectors show the same bowed-out shape as the ordinary dislocations do. This indicates that these dislocations are glissile and not locked at room temperature. It agrees with the suggestion of Girshick and Vitek (1995) and Panova and Farkas (1995) that they have a planar

core at low temperatures. In contrast with the results of Court *et al.* (1990), ordinary dislocations are very mobile at room temperature, in accordance with the work of Farenc and Couret (1993). Because of their great number and high mobility, it may be concluded that ordinary dislocations control the flow stress if their orientation factor is high enough. Thus, the following discussion is based mainly on the properties of ordinary dislocations.

The literature offers three models to explain the curly shape of ordinary dislocations, which are discussed in turn.

(1) Viguier *et al.* (1995) and Louchet and Viguier (1995) assume that neighbouring segments of ordinary screw dislocations cross-slip on different $\{111\}$ planes and bow out on them. The points linking these segments are aligned almost exactly in screw orientation. They cannot move together with the dislocations so that they form obstacles. The dislocations move very jerkily by pushing the pinning links along the dislocations in the direction of the Burgers vector to form long mobile segments, which spread very quickly.

The present observations are not in accordance with this model as the obstacles are not exactly aligned along the screw orientation. Also, obstacles occur along all types of dislocation, including edge dislocations. While jogs in edge dislocations may impede the dislocation motion, too, leading to bowed-out segments, edge dislocations cannot cross-slip, which is a prerequisite for the formation of pinning agents according to the pinning–unzipping model. However, the different behaviours of jogs on screw and edge dislocations could be one reason for the different mobilities of both, in addition to the different lattice friction processes discussed below. In the present experiments, the obstacle distance l is independent of the character of the dislocations. In addition, the stereo images do not show neighbouring segments bowing out on different crystallographic planes but mostly on parallel planes.

The discussed model cannot be used to explain the flow stress anomaly. In the two post mortem studies including data on the temperature dependence of the obstacle distances (Viguier *et al.* 1995, Sriram *et al.* 1997), the obstacle distances l decrease with increasing temperature up to 770 K but increase again at 870 K. However, the peak stress of the flow stress anomaly is at 870 K in the paper by Viguier *et al.* (1995), and at 1100 K in the study by Sriram *et al.* (1995), that is the temperature of the maximum obstacle distance is at least 100 K lower than that of the flow stress maximum. In the present work, the obstacle distances are the same for room temperature and 665 K. The dislocations are smoothly bent and move viscosely at temperatures above about 850 K, that is the pinning model no longer operates in the range of the flow stress anomaly.

(2) Very recently, Sriram *et al.* (1997) carefully investigated the spatial arrangement of the ordinary dislocations by post mortem electron microscopy. They found the individual segments bowing out on parallel planes and the cusps not strictly aligned in screw direction. Sriram *et al.* assumed that this structure of the dislocations is formed by the double-cross-slip-mechanism as originally suggested by Gilman and Johnston (1962), that is all cusps in the dislocations correspond to jogs of a spectrum of heights ranging from the atomic height up to a maximum height that is determined by the dipole opening criterion. These experimental observations are in accordance with most of the features of the microstructure of the resting dislocations at low temperatures in the present study. Deep cusps or the trailing of dipoles suggest that the ordinary screw dislocations have many jogs. However, cusps were also observed in mixed and edge dislocations as proven by

figure 4. As discussed under (1), edge dislocations cannot cross-slip to form these jogs.

The kinematic behaviour of dislocations presented in figure 5 does not agree with the fact that jogs are the dominating obstacles on screw dislocations. Figure 15(a) shows a scheme of the conservative motion of large jogs along the screw dislocations. These jogs can glide along the horizontal lines parallel to the Burgers vector. The numbers mark consecutive stages. The motion leads to long segments (stage 4) with very large bow-outs, before the configuration becomes unstable. This mechanism was identified in *in-situ* straining experiments on NiAl single crystals at room temperature by Messerschmidt *et al.* (1997). Such long segments form only by a jog mechanism, in contrast with a precipitation-hardening mechanism outlined in figure 15(b). Here, the dislocation segment moving after an obstacle is overcome has a high probability of contacting the next obstacle after sweeping an area A , which is approximately equal to the square of the obstacle distance l . Afterwards, the advanced segment spreads sideways like a kink in the Peierls model. The strongly bowed-out segments typical of the mechanisms with conservative jog motion are

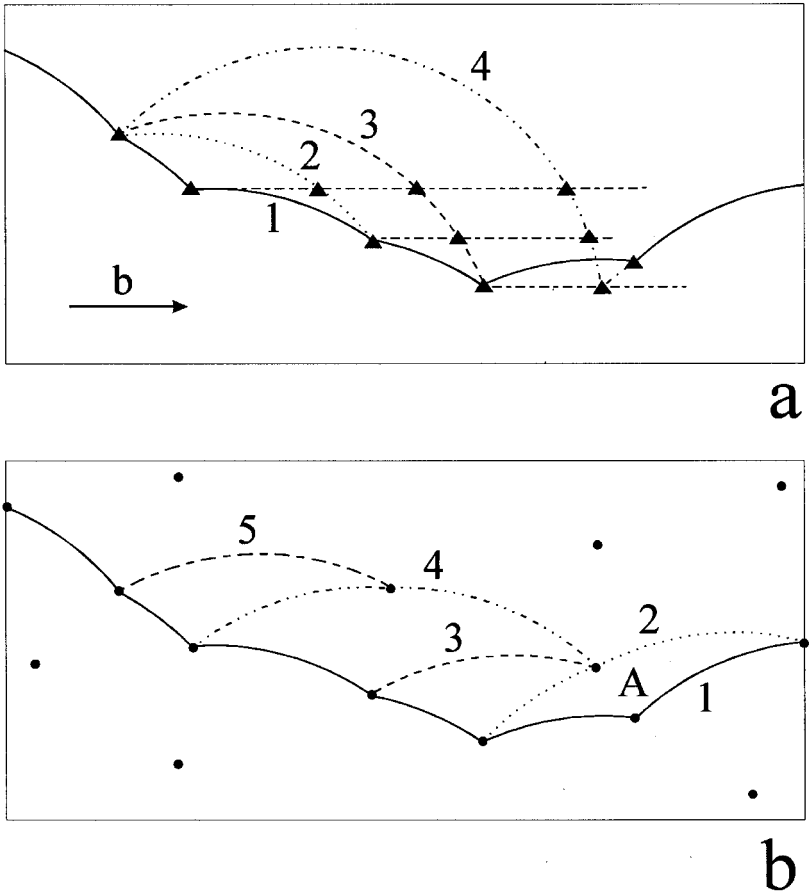


Figure 15. Schematic drawing of the kinematic behaviour of dislocations (a) in the model of conservative jog motion along screw dislocations and (b) in the model of precipitation hardening: (\blacktriangle), positions of jogs; (\bullet), positions of precipitates.

not observed in TiAl. It was assumed by Sriram *et al.* (1997) that the weak cusps correspond to elementary jogs or jogs of small height which emit or absorb vacancies during their motion. This would lead to a continuous motion of the weak cusps in forward direction, which had not been observed in the video recordings, either.

Thus, while the double-cross-slip mechanism proposed by Sriram *et al.* (1997) to control the mobility of ordinary dislocations in TiAl may explain most of the features of the resting dislocations as observed also in post mortem studies, it fails to explain the kinematic behaviour of dislocations in the *in-situ* experiments at room temperature. In no case does it explain the flow stress anomaly by the same arguments as described in (1) for the model by Louchet and Viguier (1995).

(3) Almost all experimental results can be interpreted consistently if it is assumed that during the deformation between room temperature and about 700 K, in addition to deep cusps at high jogs, the weak cusps in the dislocations result from an interaction with spatially localized obstacles, that is, probably small precipitates. The main arguments are the following.

- (a) While the shape of resting ordinary dislocations is frequently described as 'rectilinear screw dislocations' (for example Farenc and Couret (1993)), ordinary dislocations have a curly shape, with segments bowing out between obstacles distributed on the slip plane as in figure 1 and 3.
- (b) The weak cusps are certainly not jogs, but localized obstacles, since they appear on edge dislocations (figure 4) and on superdislocations (figure 2), too. The curly shape was also observed by Farenc *et al.* (1993) on twinning partial dislocations. These dislocations are not able to cross-slip on $\{111\}$ planes to form jogs.
- (c) The obstacle distance l is independent of the character and type of dislocations and of the temperature as listed in table 1.
- (d) The frequency distribution of the obstacle distances in figure 6 is similar to the theoretical distribution for precipitation hardening (Appel *et al.* 1982). The shift of the maximum of the experimental curve was also observed in other materials showing precipitation hardening (Messerschmidt 1993). The distribution in TiAl is at variance with the exponential distribution assumed for the model of Louchet and Viguier (1995, figure 2).
- (e) This view of the extrinsic nature of the obstacles is supported by the dynamic behaviour of dislocations. At low velocities, the dislocations overcome the obstacles individually. As demonstrated in figure 5, they advance small segments in forward direction, which afterwards spread sideways. This has already been discussed with respect to figure 15(b) and was also observed in computer simulations by Zaitsev and Nadgornyi (1977). The individual jumps are jerky and cannot be resolved by the video recordings (two stages in the same frame of figure 5(d)). At higher velocities, the dislocation motion becomes jerky on a larger scale owing to the increasingly athermal character. Thus, the jerky motion does not necessarily point to a locking-unlocking mechanism but is an inherent feature of precipitation hardening, too.

In the following, some quantitative estimates are made regarding the precipitation-hardening mechanism. It is assumed that the precipitates are oxide particles. The present material has a relatively low O content of 750 at.ppm. According to

Menand *et al.* (1996), the solubility limit of O in γ -TiAl is about 250 at.ppm. The remaining part should be precipitated. At present, it is not yet clear whether the precipitates are Al_2O_3 , TiO_2 or a mixed oxide such as the H phase (Blanche *et al.* 1994). TiO_2 fits quite well to the TiAl lattice. The O content strongly influences the yield stress (Huang and Hall 1991) as well as the relative activity of the different deformation mechanisms. While Morris (1996) assumed that O gives rise to solution hardening, Kad and Fraser (1994) observed some precipitates along grown-in dislocations. In a recent study, Wiezorek and Fraser (1998) proved that the precipitates along dislocations in specimens of high O content (2900 at.ppm) are enriched with O. Although using sophisticated methods of electron microscopy, these workers did not give more details about the structure of the particles about 10 nm wide. The obstacle distances of about 100 nm listed in table 1 of the present study are much too large for individual O atoms acting as obstacles. On the assumption that the precipitates are distributed homogeneously, their volume fraction f will be of the order of magnitude of 1000 ppm. For strong obstacles, the volume fraction, the average diameter $\langle w \rangle$ of the particles and their distance l along the dislocations are related by

$$\langle w \rangle = l \left(\frac{6f}{\pi} \right)^{1/2}. \quad (3)$$

With $l \approx 100$ nm from table 1, the average diameter becomes $\langle w \rangle \approx 4$ nm. Particles of this small size, being a factor of two to three smaller than those of Wiezorek and Fraser (1998) and, being of low concentration, are difficult to detect, particularly if they are coherent like TiO_2 and approximately of the same lattice constant. It is therefore not surprising that they have not yet been proven.

The activation volume V measured in macroscopic tests is related to the obstacle distance l and the size by $V = \frac{2}{3} l b d$, where the factor of $\frac{2}{3}$ results from the stress dependence of l applying Friedel statistics, $b = b_0 = 0.282$ nm is the absolute value of the Burgers vector of ordinary dislocations, and d is the so-called activation distance. The latter is the distance in forward direction between the stable position of the dislocation in front of the obstacle and the labile position after the dislocation has passed it. It should be a fraction of the obstacle width $\langle w \rangle$. Using again $l \approx 100$ nm from table 1 and $V = 13.5 \text{ nm}^3$ from table 3, d turns out to be about 0.7 nm, or $2.5b$. This fits well the estimated obstacle width of 4 nm. The small value of d indicates that the equilibrium position of the dislocations waiting for thermal activation is near the tip of the interaction potential. This corresponds to a stress not much smaller than the athermal flow stress of the obstacle array. The value of d is somewhat larger than those in other precipitation-hardened materials (Messerschmidt 1993). The activation volume measured here at room temperature is larger than that determined from the paper, for example, by Kawabata *et al.* (1985) and Inui *et al.* (1997) on single-phase γ -TiAl as well as, for example, by Appel *et al.* (1995) and Morris (1996) on two-phase Ti–Al.

The stress τ_e listed in table 2, corresponding to the dislocation bowing, can be compared with the macroscopic flow stress in table 3. τ_e was determined using the theoretical elastic constants of Fu and Yoo (1990). Very similar results are obtained using the experimental constants measured by He *et al.* (1995). The values of τ_e are the same for ordinary screw and mixed dislocations as well as for screw superdislocations. As the line tension of the superdislocations with $\{101\}$ Burgers vector is about four times that of ordinary dislocations, superdislocations bow out much

less than ordinary dislocations do under the same stress. It is important to note that the bowing of the dislocation segments only slightly relaxes after the specimens are unloaded. This indicates that a frictional stress τ_{fr} acts on the dislocations, which prevents the relaxation and which is only slightly smaller than τ_e . Frictional stresses for ordinary dislocations were calculated, for example, by Simmons *et al.* (1997) using the embedded-atom method. These stresses are high for screw dislocations, intermediate for 60° dislocations, and low for 30° and edge dislocations. This may be another reason why edge dislocations are more mobile than screw dislocations so that the latter dominate the dislocation structures.

In addition to the stress components τ_e and τ_{fr} , a long-range internal stress component, τ_i contributes to the flow stress. For a homogeneous distribution of parallel dislocations, τ_i is given by Taylor hardening according to

$$\tau_i \approx 0.5\mu b\rho^{1/2}, \quad (4)$$

where $\mu = 70$ GPa is the shear modulus, again taken from the work of Fu and Yoo (1990). An intermediate dislocation density of $\rho = 2 \times 10^{13} \text{ m}^{-2}$ from § 3.1 yields $\tau_i \approx 44$ MPa. Thus, the total resolved yield stress estimated from the microstructure

$$\tau_0 = \tau_e + \tau_{fr} + \tau_i \approx 2\tau_e + \tau_i \quad (5)$$

will be about 125 MPa. With the stress value from table 3, the macroscopic resolved yield stress $\tau_0 = \sigma_0/\alpha$ is about 60 MPa. Thus, the stress components resulting from the dislocations bowing out between obstacles, the frictional stress and the long-range athermal stress can fully explain the macroscopic yield stress. With rising temperature, thermal activation becomes more and more important. This leads to a decreasing contribution of τ_e to the flow stress and, accordingly, to a weaker bowing of the dislocation segments between the precipitates, as observed in figure 8. Finally, the precipitates are overcome spontaneously and no longer act as obstacles as in figure 9.

A very similar behaviour of dislocations was observed by Häussler *et al.* (1997) in two-phase Ti–Al materials, where the obstacle distance of about 150 nm was slightly larger than in the present material. This may be due to the gettering effect of the α_2 phase observed, for example, by Vasudevan *et al.* (1989b) and Menand *et al.* (1996). The higher flow stress of the two-phase materials is certainly due to the athermal contributions by the grain and lamellae structures, which is expressed in the Hall–Petch relationships involving the grain size or lamellae width (Vasudevan *et al.* 1989a, Mercer and Soboyejo 1996).

5.2. High temperatures

In the present study, the high temperatures applied are in the range of the flow stress anomaly. As described in § 3.2, the behaviours of both ordinary and superdislocations greatly differ from those at room temperature. While, at room temperature, superdislocations with $\langle 101 \rangle$ Burgers vectors are flexible under load and not locked, at high temperatures, they show straight segments in the three $\langle 110 \rangle$ directions on the $\{111\}$ glide plane, preferentially in $\langle 110 \rangle$ orientation as in figure 12. A high Peierls stress in the three closed-packed orientations was suggested in a computer simulation study by Rao *et al.* (1995) although the core should be planar in the two mixed orientations. The motion of superdislocations has never been recorded in *in-situ* experiments. Although the different behaviours of superdislocations at room

temperature and at high temperatures may explain the flow stress anomaly, the latter observation and the small number of superdislocations suggest that they do not play an important role in the high-temperature deformation of γ -TiAl, at least under the conditions of the *in-situ* experiments.

Above about 700 K, the dominating ordinary dislocations no longer bow out between localized obstacles. This is at variance with post mortem investigations by Viguier *et al.* (1995) and Sriram *et al.* (1997) who observed curly ordinary dislocations up to about 900 K, which might be an artefact of post mortem electron microscopy. Dislocations which at high temperatures move without being impeded by localized obstacles may again assume a bowed-out shape in the field of internal stresses after cooling. In the *in-situ* experiments, the ordinary dislocations are created instantaneously in an avalanche, which had already been observed in earlier *in-situ* experiments, as reviewed by Molénat *et al.* (1997). If they move again, they are smoothly bent as shown in figure 10, moving in a viscous way, similarly to NiAl (Messerschmidt *et al.* 1997). This had not been observed before in TiAl. It clearly contradicts the models of the flow stress anomaly of Louchet and Viguier (1995) and Sriram *et al.* (1997), as pointed out in the previous section. First, the dislocation segments no longer show the curly shape and, second, the dislocations move continuously and not in the proposed pinning–unzipping mode. As demonstrated in figure 11, the dislocations are not confined to their slip planes, indicating that climb is involved. This view is supported by the formation of helical dislocation structures in two-phase Ti–Al during *in situ* heating experiments (Appel *et al.* 1994). The importance of diffusion processes for the understanding of the high-temperature behaviour of TiAl was also stressed by Appel *et al.* (1997). Climb requires lattice diffusion of both atomic species. According to Brossmann *et al.* (1994) and Schaefer and Badura-Gergen (1996), the formation and migration energies of vacancies in TiAl are 1.4 eV and 1.6 eV respectively. Similar data follow from the most recent diffusion study by Herzig *et al.* (1998) (formation energy of the Ti vacancy; about 1 eV; formation energy of the Al vacancy; 1.5 eV; respective migration energies, 1.5 eV and 1.2 eV). Thus, these vacancies are present and mobile in the temperature range around the flow stress maximum. In addition, TiAl contains very high concentrations of antisite defects. In FeAl, the properties of thermal vacancies, the internal friction and the kinetics of establishing the flow stress anomaly are closely related as observed by Schaefer *et al.* (1997). Recently, at 10 Hz, a peak in the internal friction of γ -TiAl at 1080 K as well as a strong increase in the background friction above 1000 K were found by Hirscher *et al.* (1998), supporting this view also for TiAl.

Since the low-temperature mechanism of precipitation hardening ceases to operate above 850 K, an additional process must cause the increase or at least the constancy of the flow stress in the range of the anomaly. Here, it is assumed that diffusion-controlled processes give rise to an additional friction impeding the motion of dislocations owing to the formation of atmospheres around them. The atmosphere formation may be superimposed with climb. However, climb usually results in recovery and does not induce additional friction. The atmospheres may form from solute impurities as proposed by Molénat *et al.* (1997) and Christoph *et al.* (1997) to cause strain-ageing effects. The frictional stress τ_f shows a maximum at a certain dislocation velocity v , which has been described in detail by Hirth and Lothe (1982) and drawn schematically in figure 16. While, at low velocities, the atmospheres can easily follow the dislocation motion, at high velocities, the dislocations break away

from the atmospheres. The interaction has a maximum at a certain intermediate velocity v_c . This dependence explains the coexistence of dislocations moving very fast in an avalanche and such moving viscously at low velocities. Applying the theory of the Cottrell effect, the stress contribution at the maximum can be estimated by (Hirth and Lothe 1982, equation (18-83))

$$\sigma_{\max} \approx \frac{17c_0\beta}{b^4}, \quad (6)$$

with $\beta = (\mu b/3\pi) [(1+\nu)/(1-\nu)](v_s - v_m)$. c_0 is the concentration of the defects forming the atmospheres, μ is the shear modulus as in equation (4), ν is Poisson's ratio, and v_s and v_m are the volumes of the defect and the matrix atoms respectively. Using the data $\nu = 0.226$ (He *et al.* 1995), $v_s/v_m = 1.1$ and $v_m = b^3$, a defect concentration c_0 of about 1000 ppm is necessary to yield $\sigma_{\max} \approx 20$ MPa. This agrees with the experimental results reviewed by Kubin and Estrin (1991) that in most materials there exist some 1000 ppm of impurities if strain-ageing effects are observed. The material of the present study does not contain such high concentrations of impurities. It has been shown by Lerf and Morris (1994) for $L1_2$ Al_3Ti , and by Popille *et al.* (1996) for $B2$ Ti_2AlX with $X = Nb, Mo$ and $MoNb$ that the strain-ageing effects can also be caused by intrinsic point defects, vacancies and antisite atoms, owing to a non-stoichiometric composition. Binding energies have been calculated between the point defects and the dislocations (for example Schroll and Gumbsch (1998)). They may be positive or negative and are usually below 1 eV. However, in a particular configuration of an antisite defect in the core of a dislocation in NiAl, the dislocation reconstructs locally so that the binding energy is larger

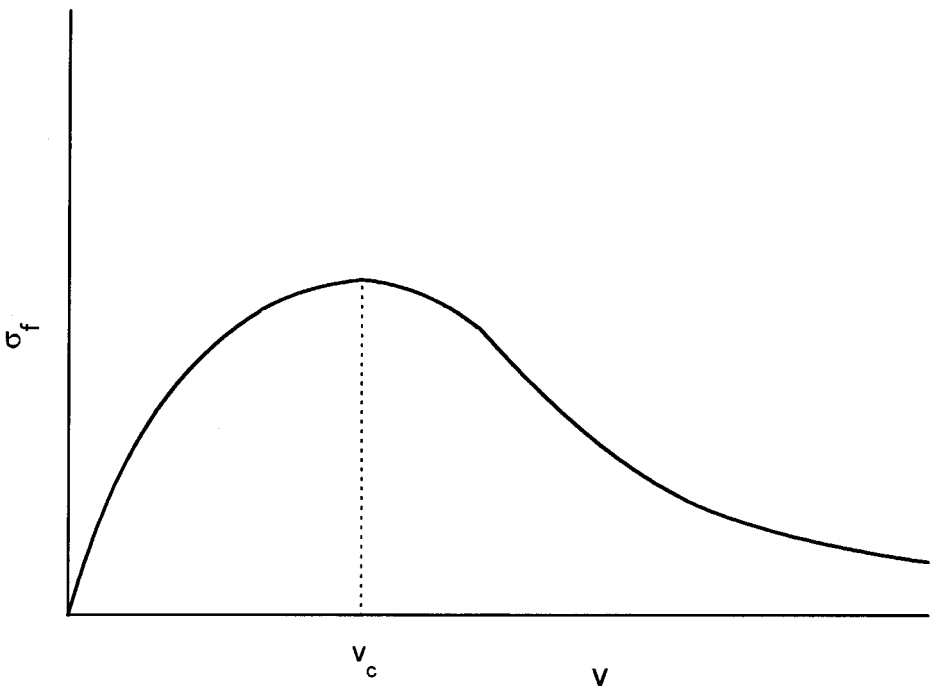


Figure 16. Schematic plot of the dependence of the frictional stress σ_f , arising from atmospheres around dislocations, on the glide velocity v .

than the formation energy of the defect. Thus, the energy of the dislocation including the defect is lower than that without it. Messerschmidt *et al.* (1998) used this result to propose a new model of the dislocation motion in an intermetallic alloy at high temperatures, assuming that the configuration with the lowest energy of a dislocation may generally require a certain concentration of intrinsic point defects, in addition to other structural and chemical disorder of the material. The moving dislocations may drag these intrinsic defect clouds in exactly the same way as Cottrell or other impurity atmospheres to cause an additional friction of the dislocations, which results in a viscous dislocation motion. These clouds may be restricted to a region close to the core of the dislocations, but diffusion is necessary to move the clouds together with the dislocations.

Again, using the theory of the Cottrell effect, the dislocation velocity v_c at the maximum stress can be related to the diffusion coefficient of the defects forming the atmospheres by (Hirth and Lothe 1982, equation (18-82))

$$v_c = \frac{4DkT}{\beta}, \quad (7)$$

where D is the diffusion coefficient, and k and T have their usual meanings. Applying the Orowan relation between the dislocation velocity v and the strain rate $\dot{\epsilon}$, that is

$$\dot{\epsilon} = \rho_m b v, \quad (8)$$

the necessary diffusion coefficient can be estimated. ρ_m is the mobile dislocation density. Using the appropriate data $\dot{\epsilon} = 10^{-5} \text{ s}^{-1}$, $\rho_m = 2 \times 10^{13} \text{ m}^{-2}$ and the temperature of $T = 1000 \text{ K}$ of the flow stress maximum, the diffusion coefficient of the defects forming the atmospheres should be about $D = 2.4 \times 10^{-19} \text{ m}^2 \text{ s}^{-1}$. This value fits very well the extrapolated diffusion data of Ti in TiAl (Schaefer and Badura-Gergen 1996, Herzig *et al.* 1998). It is higher than the diffusion coefficient of Al (Herzig *et al.* 1998). The present estimates are intended to show that a concentration of intrinsic point defects belonging to the equilibrium state of dislocations in intermetallics may cause strain-ageing effects sufficiently strong to contribute to the flow stress anomaly. They neither prove the model nor identify the responsible defect. Further theoretical and experimental work is necessary.

The assumption that point-defect atmospheres control the dislocation mobility in the range of the flow stress anomaly is consistent with the dependence of the strain-rate sensitivity I on the strain rate $\dot{\epsilon}$. If figure 16 is replotted as σ_f against $\ln \dot{\epsilon}$, the slope is equal to the strain-rate sensitivity I . Below v_c , I is positive. It decreases with increasing velocity and becomes zero at v_c . This behaviour is expressed in the 'inverse' curvature of the stress relaxation curves in figure 13 and in the decrease in I with increasing strain rate in figure 14. A similar effect was observed by Morris and Lipe (1997, figure 6) during the creep of two-phase Ti–Al. In figure 14, the increase in I with increasing strain can be explained by the decreasing dislocation velocity owing to the rise in the dislocation density. The viscous motion of the dislocations in the *in-situ* experiments corresponds to this range of positive strain-rate sensitivity. At high dislocation velocities, the strain-rate sensitivity becomes negative, leading to plastic instabilities, which may occur in TiAl at intermediate temperatures (for example Dong *et al.* (1992)). In the *in-situ* experiments, the instantaneous formation and motion of ordinary dislocations during the first loading belong to this range. This model explains the observation that the flow stress anomaly becomes more pronounced the more the Al content increases beyond 50%, since

the structural disorder due to the deviation from stoichiometry may be involved in the formation of the atmospheres. Stress relaxation curves with 'inverse' curvature were also observed in MoSi₂, showing a flow stress anomaly, but they do not occur in NiAl, which does not show an anomaly (Messerschmidt *et al.* 1998). 'Non-logarithmic' stress relaxation curves were also observed in TiAl at room temperature by Bonneville *et al.* (1997). The nature of this effect is different from the present effect.

As described in § 4, only a small part of the stress relaxes during the stress relaxation tests. This is a qualitative indication that a great part of the flow stress is of athermal nature, which seems to contradict the view that the dislocation motion is controlled by the thermally activated processes of point-defect atmospheres. However, it has already been pointed out by Hirth and Lothe (1982) that, according to equation (8), a reduced dislocation mobility leads to an increase in the mobile dislocation density ρ_m , which in turn results in an increased athermal component of the flow stress. Unfortunately, to the present authors' knowledge, there are no representative data available for dislocation densities in TiAl in the different temperature ranges.

The *in-situ* experiments in the intermediate-temperature range, described in § 3.2, demonstrate that the transition from the low-temperature mechanism of the thermally activated overcoming of obstacles to the high-temperature mechanism involving lattice diffusion occurs between about 700 and 870 K. There is probably a wide range where both mechanisms are superimposed.

§6. CONCLUSIONS

- (1) *In-situ* straining experiments in a high-voltage electron microscope yield important information on the microprocesses of deformation. In γ -TiAl at room temperature, ordinary dislocations bow out under load on parallel planes, with the cusps not being aligned exactly along screw orientations. Superdislocations under load show a similar shape, that is they are flexible and not locked.
- (2) This shape of the dislocations as well as their dynamic behaviour can best be explained by a precipitation-hardening mechanism controlling the dislocation motion between room temperature and about 700 K. This mechanism, together with lattice friction and Taylor hardening, semiquantitatively explains the macroscopic flow stress as well as the strain-rate sensitivity.
- (3) Above about 850 K, ordinary dislocations move in either an unstable or a viscous way. This may be interpreted by the diffusion-controlled formation of atmospheres, which cause an additional friction by strain-ageing effects and are thus responsible for the flow stress anomaly. This conclusion is in agreement with the decrease in the strain-rate sensitivity with increasing strain rate.
- (4) As the concentration of impurities is too low to account for the observed strain-ageing effects, a new model is proposed which assumes that the configuration of lowest energy of a dislocation in an intermetallic alloy requires a certain concentration of intrinsic point defects and that these atmospheres move together with the dislocations.

ACKNOWLEDGEMENTS

The authors are grateful to the reviewers which, by their comments, helped very much to improve the manuscript. The authors also wish to thank the staff of the

Halle high-voltage electron microscope for excellently maintaining the instrument as well as for technical help. Financial support by the Deutsche Forschungsgemeinschaft and the ARC programme of the British Council and the Deutsche Akademische Austauschdienst is gratefully acknowledged.

REFERENCES

- AINDOW, M., CHAUDHURI, K., DAS, S., and FRASER, H. L. 1990, *Scripta metall. mater.*, **24**, 1105.
- APPEL, F., LORENZ, U., OEHRING, M., SPARKA, U., and WAGNER, R., 1997, *Mater. Sci. Engng.* **A233**, 1.
- APPEL, F., LORENZ, U., SPARKA, U., and WAGNER, R., 1994, *Strength of Materials*, edited by H. Okawa, M. Maruyama, S. Takeuchi and M. Yamaguchi (Sendai: Japan Institute of Metals), p. 341.
- APPEL, F., MESSERSCHMIDT, U., NADGORNYI, E. M., and ZAITSEV, S. I., 1982, *Mater. Sci. Engng.* **52**, 69.
- APPEL, F., SPARKA, U., and WAGNER, R., 1995, *High Temperature Ordered Intermetallic Alloys VI*, Materials Research Society Symposium Proceedings, Vol. 364 (Pittsburg, Pennsylvania: Materials Research Society), 623.
- BLANCHE, G., JAOUEN, M., FLANK, A.-M., and HUG, G., 1994, *J. Phys., Paris, IV*, **4**, C9-145.
- BONNEVILLE, J., VIGUIER, B., and SPÄTIG, P., 1997, *Scripta mater.*, **36**, 275.
- BROSSMANN, U., WÜRSCHUM, R., BADURA, K., and SCHAEFER, H.-E., 1994, *Phys. Rev. B*, **49**, 6457.
- CAILLARD, D., 1995, *High Temperature Ordered Intermetallic Alloys VI*, Materials Research Society Symposium Proceedings, Vol. 364 (Pittsburg, Pennsylvania: Materials Research Society), 17.
- CAILLARD, D., COURET, A., MOLENAT, G., and CRESTOU, J., 1993, *Microsc. Microanal. Microstruct.*, **4**, 183.
- CHRISTOPH, U., APPEL, F., and WAGNER, R., 1997, *High Temperature Ordered Intermetallic Alloys VII*, Materials Research Society Symposium Proceedings, Vol. 460 (Pittsburg, Pennsylvania: Materials Research Society), 207.
- COURT, S. A., VASUDEVAN, V. K., and FRASER, H. L., 1990, *Phil. Mag. A*, **61**, 141.
- DONG, Z., LIMING, W., DUNXU, Z., MEI, Y., and QIGONG, C., 1992, *J. Mater. Sci. Lett.*, **11**, 1026.
- FARENC, S., CALLIARD, D., and COURET, A., 1991, *Proceedings of the Sixth Japan Institute of Metals International Symposium on Intermetallic Compounds, Structure and Mechanical Properties* (Sendai: Japan Institute of Metals) p. 791.
- FARENC, S., and COURET, A., 1993, *High Temperature Ordered Intermetallic Alloys V*, Materials Research Society Symposium Proceedings, Vol. 288 (Pittsburg, Pennsylvania: Materials Research Society), 465.
- FARENC, S., COUJOU, A., and COURET, A., 1993, *Phil. Mag. A*, **67**, 127.
- FU, C. L., and YOO, M. H., 1990, *Phil. Mag. A*, **62**, 159.
- GILMAN, J. J., and JOHNSTON, W. G., 1962, *Solid St. Phys.*, **13**, 147.
- GIRSHICK, A., and VITEK, V., 1995, *High Temperature Ordered Intermetallic Alloys VI*, Materials Research Society Symposium Proceedings, Vol. 364 (Pittsburg, Pennsylvania: Materials Research Society), 145.
- GREENBERG, B. A., ANTONOVA, O. V., INDEBAUM, V. N., KARKINA, L. E., NOTKIN, A. B., PONOMAREV, M. V., and SMIRNOV, L. V., 1991, *Acta metall. mater.*, **39**, 233.
- HÄUSSLER, D., BARTSCH, M., MESSERSCHMIDT, U., AINDOW, M., and JONES, I. P., 1995, *Inst. Phys. Conf. Ser.*, **147**, 463.
- HÄUSSLER, D., MESSERSCHMIDT, U., BARTSCH, M., APPEL, F., and WAGNER, R., 1997, *Mater. Sci. Engng.* **A233**, 15.
- HE, Y., SCHWARZ, R. B., MIGLIORI, A., and WANG, S. H., 1995, *J. Mater. Res.*, **10**, 1187.
- HERZIG, CHR., PRZEORSKI, T., and MISHIN, Y., 1998, *Intermetallics* (submitted).
- HIRSCHER, M., SCHAIBLE, D., KRONMÜLLER, H., OEHRING, M., and APPEL, F., 1998, *Spring Meeting of the German Physical Society*, Regensburg, 23-27 March 1998 (German Physical Society), abstract M7.10.
- HIRTH, J. P., and LOTHE, J., 1982, *Theory of Dislocations* (New York: Wiley).
- HISHINUMA, A., NAKATA, K., FUKAI, K., AMEYAMA, K., and TOKIZANE, M., 1993, *J. nucl. Mater.*, **199**, 167.

- HUANG, S. C., and HALL, E. L., 1991, *Metall. Trans. A*, **22**, 427.
- HUG, G., LOISEAU, A., and VEYSSIÈRE, P., 1988, *Phil. Mag. A*, **57**, 499.
- INUI, H., MATSUMORO, M., WU, D.-H., and YAMAGUCHI, M., 1997, *Phil. Mag. A*, **75**, 395.
- KAD B. M., and FRASER, H. L., 1994, *Phil. Mag. Lett.*, **70**, 211.
- KAWABATA, T., KANAI, T., and IZUMI, O., 1985, *Acta metall.*, **33**, 1355.
- KEAR, B. H., and WILSDORF, H. G. F., 1962, *Trans. AIME*, **224**, 382.
- KUBIN, L. P., and ESTRIN, Y., 1991, *J. Phys., Paris, III*, **1**, 929.
- LERF, R., and MORRIS, D. G., 1994, *Acta metall. mater.*, **42**, 1091.
- LOUCHET, F., and VIGUIER, B., 1995, *Phil. Mag. A*, **71**, 1313.
- MENAND, A., HUGUET, A., and NÉRAC-PARTAIX, A., 1996, *Acta mater.*, **44**, 4729.
- MERCER, C., and SOBOYEJO, W. O., 1996, *Scripta mater.*, **35**, 17.
- MESSERSCHMIDT, U., 1993, *Z. Metallk.*, **84**, 393.
- MESSERSCHMIDT, U., and APPEL, F., 1976, *Ultramicroscopy*, **1**, 223.
- MESSERSCHMIDT, U., and BARTSCH, M., 1994, *Ultramicroscopy*, **56**, 163.
- MESSERSCHMIDT, U., BARTSCH, M., GUDER, S., HÄUSSLER, D., HAUSHÄLTER, R., and YAMAGUCHI, M., 1998, *Intermetallics* (to be published).
- MESSERSCHMIDT, U., BARTSCH, M., HÄUSSLER, D., AINDOW, M., HATTENHAUER, R., and JONES, I. P., 1995, *High Temperature Ordered Intermetallic Alloys VI*, Materials Research Society Symposium Proceedings, Vol. 364 (Pittsburg, Pennsylvania: Materials Research Society), p. 47.
- MESSERSCHMIDT, U., HAUSHÄLTER, R., and BARTSCH, M., 1997, *Mater. Sci. Engng.* **A234–A236**, 822.
- MOLÉNAT, G., COURET, A., and CAILLARD, D., 1997, *Mater. Sci. Engng.* **A234–A236**, 660.
- MORRIS, M. A., 1996, *Intermetallics*, **4**, 417.
- MORRIS, M. A., and LIPE, T., 1997, *Intermetallics*, **5**, 329.
- PANOVA, J., and FARKAS, D., 1995, *High Temperature Ordered Intermetallic Alloys VI*, Materials Research Society Symposium Proceedings, Vol. 364 (Pittsburg, Pennsylvania: Materials Research Society), p. 151.
- POPILLE, F., KUBIN, L. P., DOUIN, J., and NAKA, S., 1996, *Scripta mater.*, **34**, 977.
- RAO, S., WOODWARD, C. SIMMONS, J., and DIMIDUK, S., 1995, *High Temperature Ordered Intermetallic Alloys VI*, Materials Research Society Symposium Proceedings Vol. 364 (Pittsburgh, Pennsylvania: Materials Research Society) p. 129.
- SCATTERGOOD, R. O., and BACON, D. J., 1975, *Phil. Mag. A*, **31**, 179.
- SCHAEFFER, H.-E., and BADURA-GERGEN, K., 1996, *Defects Diffusion Forum*, **143–147**, 193.
- SCHAEFFER, H.-E., DAMSON, B., WELLER, M., ARZT, E., and GEORGE, E. P., 1997, *Phys. Stat. sol. (a)*, **160**, 531.
- SCHROLL, R., and GUMBSCH, P., 1998, *Phys. Stat. sol. (a)*, **166**, 475.
- SIMMONS, J. P., MILLS, M. J., and RAO, S. I., 1995, *High Temperature Ordered Intermetallic Alloys VI*, Materials Research Society Symposium Proceedings, Vol. 364 (Pittsburg, Pennsylvania: Materials Research Society), p. 137.
- SIMMONS, J. P., RAO, S. I., and DIMIDUK, D. M., 1997, *Phil. Mag. A*, **75**, 1299.
- SRIRAM, S., DIMIDUK, D. M., HAZZLEDINE, P. M., and VASUDEVAN, V. K., 1997, *Phil. Mag. A*, **76**, 965.
- SRIRAM, S., VASUDEVAN, V. K., and DIMIDUK, D. M., 1995, *High Temperature Ordered Intermetallic Alloys VI*, Materials Research Society Symposium Proceedings, Vol. 364 (Pittsburg, Pennsylvania: Materials Research Society), p. 647.
- VASUDEVAN, V. K., COURT, S. A., KURATH, P., and FRASER, H. L., 1989a, *Scripta metall.*, **23**, 467.
- VASUDEVAN, V. K., STUECKE, M. A., COURT, S. A., and FRASER, H. L., 1989b, *Phil. Mag. A*, **59**, 299.
- VIGUIER, B., HEMKER, K. J., BONNEVILLE, J., LOUCHET, F., and MARTIN, J.-L., 1995, *Phil. Mag. A*, **71**, 1295.
- VITEK, V., 1992, *Prog. Mater. Sci.*, **36**, 1.
- WIEZOREK, J. M. K., and FRASER, H. L., 1998, *Phil. Mag. A*, **77**, 661.
- YAMAGUCHI, M., INUI, H., KISHIDA, K., MATSUMURO, M., and SHIRAI, Y., 1995, *High Temperature Ordered Intermetallic Alloys VI*, Materials Research Society Symposium Proceedings, Vol. 364, (Pittsburg, Pennsylvania: Materials Research Society), p. 3.
- ZAITSEV, S. I., and NADGORNYYI, E. M., 1977, *Nucl. Metall.*, **20**, 707.